Dyes and Pigments 91 (2011) 33–43

Contents lists available at ScienceDirect

Dyes and Pigments

journal homepage: www.elsevier.com/locate/dyepig

Electro-optical properties of new anthracene based organic dyes for dye-sensitized solar cells

K.R. Justin Thomas [a,*], Prachi Singh [a], Abhishek Baheti [a], Ying-Chan Hsu [b], Kuo-Chuan Ho [b], Jiann T'suen Lin [c]

[a] Organic Materials Lab, Department of Chemistry, Indian Institute of Technology Roorkee, Roorkee 247 667, India
[b] Department of Chemical Engineering, National Taiwan University, Taipei 10617, Taiwan
[c] Institute of Chemistry, Academia Sinica, 115 Nankang, Taipei, Taiwan

ARTICLE INFO

Article history:
Received 19 November 2010
Received in revised form
28 December 2010
Accepted 21 February 2011
Available online 8 March 2011

Keywords:
Anthracene
Triarylamine
Benzothiadiazole
Dye-sensitized solar cell
Absorption spectra
Theoretical calculation

ABSTRACT

Dipolar compounds containing anthracene-based triarylamine donor and cyanoacrylic acid acceptor were synthesized and characterized by electro-optical measurements. The optical spectra of the dyes are dominated by a charge transfer transition. This band is red-shifted and increased in intensity on elongation of conjugation by the introduction of bithiophene or dithienylbenzothiadiazole moiety. Similarly, the oxidation potentials of the dyes are shifted anodically on extension of the conjugation attributable to the reduction in the interaction between the triarylamine and acceptor segments. Theoretical calculations revealed the charge transfer to occur between anthracene and triarylamine moieties. However, in the benzothiadiazole containing dye the charge transfer is observed between the amine and the acceptor segment. Dye-sensitized solar cells fabricated using these dyes showed moderate efficiency which is highly dependent on the nature of the conjugation bridge.

© 2011 Elsevier Ltd. All rights reserved.

1. Introduction

There is a growing demand for the development of alternate technologies for the conservation of energy due to the expectation that the fossil fuels may be consumed completely. Solar energy can be converted to electricity by photovoltaic and photoelectrochemical cells [1]. Photoelectrochemical cells commonly termed as Grätzel cells or dye-sensitized solar cells (DSSCs) are based on the sensitization of wide band gap semiconductors such as nanocrystalline anatase TiO_2 by inorganic or organic dyes capable of absorbing sun light in the entire visible region. DSSCs are considered cheap and robust alternatives to the conventional silicon-based photovoltaic devices. The efficiency of the DSSCs largely depends on the light absorbing capability of the dye while the other parameters such as electron injection and dye regeneration are also crucial. Ruthenium-based organometallic complexes developed by Grätzel and co-workers [2,3] are the most successful dyes with promising device characteristics. However, the ruthenium dyes are expensive and consequently a search is active for the development of organic dyes featuring advantageous electro-optical properties. Organic dyes are attractive due to the availability of facile synthetic methodologies and exhibition of large molar extinction coefficients when compared to the dominant ruthenium-based dyes. Organic dyes commonly feature donor–acceptor architecture with the donor being a triarylamine and a cyanoacrylic acid acceptor. Variation of the conjugating segment that links the donor and acceptor fragments have led to a huge array of dyes displaying promising energy conversion efficiencies and broader and intense incident photon-to-current efficiency (IPCE) response. Aromatic linkers such as phenyl [4,5], biphenyl [6], terphenyl [7], fluorene [8–10], coumarin [11,12], thiophene [13–17], thienothiophene [18–20], furan [21], pyrrole [22] and benzothiadiazole [23,24] have been exploited to develop dyes for DSSCs.

Anthracene-based molecular materials are known for displaying bright blue electroluminescence [25–28]. Simple 9,10-diaryl substituted anthracenes have been demonstrated as emitting materials while the incorporation of arylamine moiety enhances the hole-transporting ability of such compounds [28–31]. Even though the anthracene containing compounds have been developed successfully for applications in light-emitting diodes [25–31], thin film transistors [32–34] and constituents in bulk heterojunction solar cells [35] their use in DSSCs remain limited. Simple

* Corresponding author. Tel.: +91 1332285376; fax: +91 1332286202.
E-mail address: krjt8fcy@iitr.ernet.in (K.R. Justin Thomas).

0143-7208/$ – see front matter © 2011 Elsevier Ltd. All rights reserved.
doi:10.1016/j.dyepig.2011.02.006

anthracene-cyanoacrylic acid derivatives have been recently reported as sensitizers for DSSCs [36,37]. In a recent paper by Hagfeldt et al. [36] anthracene unit has been employed as a linker for triphenylamine donors and cyanoacrylic acid acceptors. However, to the best of our knowledge arylamines derived from anthracene have not been exploited for the construction of dyes suitable for dye-sensitized solar cells. In this paper, we present three dyes (Fig. 1) featuring thiophene, bithiophene and dithienylbenzothiadiazole linkers inserted between the anthracene-based triarylamine donor and cyanoacrylic acid acceptor units. Thiophene moiety is used to increase the electron-richness of the linking segment, on the contrary the electron-deficient benzothiadiazole unit is expected to shift the LUMO toward the cyanoacrylic anchoring segment and favour a facile charge transfer transition between the triarylamine and cyanoacrylic acid units. The *tert*-butyl groups were introduced in the anthracene nucleus for two reasons: (a) incorporation of *tert*-butyl groups are expected to improve the solubility of the dyes and (b) inhibit the aggregation between the dyes which is more pronounced in the unsubstituted anthracene derivatives [38]. It has been demonstrated in few reports that the incorporation of substituents at the 2 and/or 7-positions of the anthracene nucleus reduce the aggregation propensity [39,40]. Aggregation of dyes when anchored on the TiO_2 surface may alter the absorption and electron transfer properties which in turn may affect the performance of the DSSCs. Intermolecular interactions via the anthracene moiety in the present design will be inhibited not only due to the presence of *tert*-butyl groups but also due to the anchoring of diarylamine segment. Trigonal amine unit will also sterically forbid the approach of adjacent molecules.

Our aim is to study the role of anthracene in the donor–acceptor architecture and compare the absorption and DSSC performance parameters with the analogous dyes reported in the literature and featuring phenylene, thienyl or fluorene moieties in place of anthracene. TDDFT computations are used to rationalize the optical properties and charge transfer probability. Initial TDDFT computations revealed the localization of LUMO orbitals over the anthracene moiety and disfavouring the charge transfer necessary for electron injection to the nanocrystalline TiO_2. However, on inclusion of benzothiadiazole unit in the conjugation pathway shifted the LUMO toward the cyanoacrylic acid segment. In addition, the electron-rich oligothiophene and electron-deficient benzothiadiazole segments are expected to reduce the band gap and red-shift the absorption features. Such an improvement in optical properties is hypothesized to benefit the light harvesting properties of the dyes when used in the dye-sensitized solar cells.

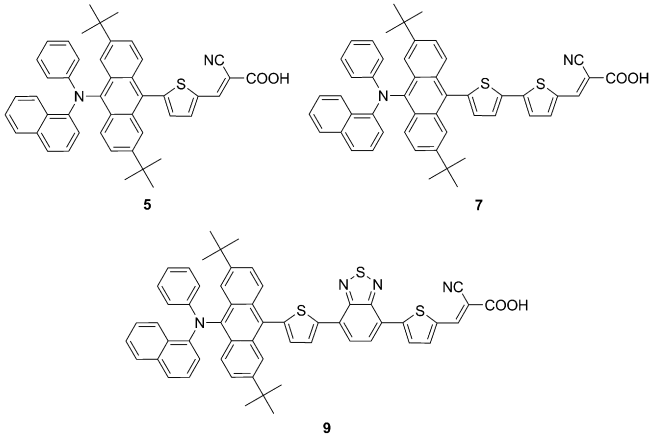

Fig. 1. Structures of the anthracene-based dyes.

2. Experimental details

2.1. Materials

All the reactions were carried out under nitrogen unless otherwise mentioned. Solvents were dried by standard procedures. All column chromatography separations were performed using silica gel (230–400 mesh) as the stationary phase. The ^1H and ^{13}C NMR spectra were measured by using Bruker AMX400 or AV400 spectrometer. Mass spectra were recorded on a JMS-700 double focusing mass spectrometer (JEOL, Tokyo, Japan). Elemental analyses were performed on a Perkin-Elmer 2400 CHN analyzer. Cyclic voltammetric experiments were performed with a CH Instruments electrochemical analyzer. All measurements were carried out at room temperature with a conventional three-electrode configuration consisting of a glassy carbon working electrode, a platinum wire auxiliary electrode, and a nonaqueous $Ag/AgNO_3$ reference electrode. The $E_{1/2}$ values were determined as $1/2(E_p^a + E_p^c)$, where E_p^a and E_p^c are the anodic and cathodic peak potentials, respectively. The potentials are quoted against the ferrocene internal standard. The solvent in all experiments was dichloromethane and the supporting electrolyte was 0.1 M tetrabutylammonium hexafluorophosphate. Electronic absorption spectra were obtained on a Cary 50 Probe UV–Visible spectrophotometer. The precursor compound **1** was obtained according to the literature procedure [26].

2.2. 2-(10-Bromo-2,6-di-tert-butylanthracen-9-yl)thiophene (**2**)

A two-neck flask was charged with magnesium turnings (0.24 g, 10 mmol) and tetrahydrofuran (50 ml) and rapidly stirred under nitrogen atmosphere. 2-Bromothiophene (1.63 g, 10 mmol) was added through the side arm cautiously *via* a syringe. After stirring for 1 h the Grignard reagent formed was transferred using a cannula to a flask containing 9,10-dibromo-2,6-di-*tert*-butylanthracene (**1**) (5.38 g, 12 mmol) and bis(triphenylphosphine)palladium dichloride (0.07 g). The mixture was heated to reflux for 24 h. At the end it was poured into iced water and the organic products formed were extracted with diethyl ether (3×50 ml). The combined organic extracts were concentrated and adsorbed on silica gel. It was purified by column chromatography by using hexane/dichloromethane mixture (5:1) as eluant. Pale yellow solid. Yield: 2.53 g (56%). ^1H NMR ($CDCl_3$, 500 MHz, ppm): δ 1.31 (s, 9 H), 1.46 (s, 9 H), 7.15–7.16 (m, 1 H), 7.27–7.30 (m, 1 H), 7.50 (dd, $J = 1.8$, 9.2 Hz, 1 H), 7.59 (dd, $J = 1.5$, 7.4 Hz, 1 H), 7.66 (dd, $J = 1.8$, 9.2 Hz, 1 H), 7.72 (d, $J = 1.8$ Hz, 1 H), 7.77 (d, $J = 9.2$ Hz, 1 H), 8.45 (d, $J = 1.8$ Hz, 1 H), 8.50 (d, $J = 9.2$ Hz, 1 H).

2.3. 2,6-Di-tert-butyl-N-(naphthalen-1-yl)-N-phenyl-10-(thiophen-2-yl)anthracen-9-amine (**3**)

A mixture of **2** (4.51 g, 10 mmol), *N*-phenylnaphthalen-1-amine (2.63 g, 12 mmol), $Pd(dba)_2$ (0.055 g, 0.02 mmol), $(t\text{-Bu})_3P$ (0.051 g, 0.02 mmol), sodium *t*-butoxide (1.44 g, 15 mmol) and dry toluene (25 ml) was heated at 80 °C for 12 h in a Schlenk flask. After the completion of the reaction it was evaporated to dryness in a rotary evaporator and the residue was adsorbed on silica gel. It was purified by column chromatography by using hexane/dichloromethane mixture (4:1) as eluant. Yellow solid. Yield: 4.78 g (81%). ^1H NMR ($CDCl_3$, 500 MHz, ppm): δ 1.07 (s, 9 H), 1.26 (s, 9 H), 6.66–6.70 (m, 2 H), 6.77–6.81 (m, 1 H), 7.05–7.12 (m, 3 H), 7.18–7.22 (m, 2 H), 7.29–7.32 (m, 1 H), 7.38–7.43 (m, 2 H), 7.45–7.52 (m, 2 H), 7.58–7.61 (m, 2 H), 7.77–7.83 (m, 2 H), 7.90 (dd, $J = 1.8$, 9.2 Hz, 1 H), 8.16–8.20 (m, 2 H), 8.30 (d, $J = 8.2$ Hz, 1 H). ^{13}C NMR ($CDCl_3$, 125 MHz, ppm): δ 150.9, 148.2, 147.5, 142.9, 135.2, 132.7, 129.4, 129.0, 128.3, 127.0, 126.8, 126.6, 126.2, 125.7, 124.9, 124.3, 123.0, 121.5, 119.7, 118.6, 116.1,

35.0, 34.9, 30.8, 30.7. FAB MS: *m/z* 589.2 [M^+]. HRMS: Calcd. for $C_{42}H_{39}NS$ 589.2803. Found: 589.2791 [M^+].

2.4. 5-(2,6-Di-tert-butyl-10-(naphthalen-1-yl(phenyl)amino) anthracen-9-yl)thiophene-2-carbaldehyde (**4**)

Compound **3** (1.18 g, 2 mmol) was dissolved in dry tetrahydrofuran (50 ml) and cooled to −70 °C. To this mixture *n*-butyl lithium (1.4 ml (1.6 M solution in *n*-hexane) 2.2 mmol) was added drop by drop for 30 min with vigorous stirring. The reaction mixture was stirred for another 90 min at this temperature and 2 ml dry dimethylformamide added at once. It was allowed to attain room temperature overnight. The resulting yellow solution was poured into ice-water and treated with saturated ammonium chloride solution briefly. It was extracted with diethyl ether (3 × 25 ml) and the combined organic extracts dried over anhydrous $MgSO_4$. Evaporation of the diethyl ether solution produced the crude aldehyde which was further purified by column chromatography on silica gel using 1:1 mixture of hexane and dichloromethane. Dark yellow solid. Yield: 0.67 g (54%). ^{1}H NMR ($CDCl_3$, 500 MHz, ppm): δ 1.12 (s, 9 H), 1.31 (s, 9 H), 6.72–6.77 (m, 2 H), 6.84 (t, J = 7.4 Hz, 1 H), 7.11–7.27 (m, 5H), 7.37 (d, J = 4.0 Hz, 1 H), 7.43–7.54 (m, 4 H), 7.62 (d, J = 8.2 Hz, 1 H), 7.75–7.85 (m, 2 H), 7.94 (dd, J = 1.8, 9.2 Hz, 1H), 8.01 (d, J = 4.0 Hz, 1 H), 8.25–8.32 (m, 2 H), 8.35 (d, J = 8.2 Hz, 1 H), 10.08 (s, 1 H). ^{13}C NMR ($CDCl_3$, 125 MHz, ppm): δ 182.9, 150.7, 148.5, 148.3, 144.8, 136.5, 131.1, 131.0, 129.1, 129.0, 128.9, 126.1, 126.0, 125.9, 125.8, 125.7, 125.6, 125.1, 124.5, 123.0, 120.6, 119.9, 119.5, 118.6, 115.3, 35.0, 30.7.

2.5. (E)-2-Cyano-3-(5-(2,6-di-tert-butyl-10-(naphthalen-1-yl (phenyl)amino)anthracen-9-yl)thiophen-2-yl)acrylic acid (**5**)

A mixture of the aldehyde **4** (0.618 g, 1 mmol), 2-cyanoacetic acid (0.102 g, 1.2 mmol), ammonium acetate (0.039 g, 0.5 mmol) and acetic acid (5 ml) was refluxed for 8 h. The resulting dark red solution was poured into water. The solid was filtered and thoroughly washed with water and hexane/diethyl ether mixture. It was recrystallized from dichloromethane/hexane mixture. Red powder. Yield: 0.47 g (69%). ^{1}H NMR (DMSO-d_6, 500 MHz, ppm): δ 0.99 (s, 9 H), 1.21 (s, 9 H), 6.51 (d, J = 7.6 Hz, 1 H), 6.58 (d, J = 7.6 Hz, 1 H), 6.82 (t, 7.4 Hz, 1 H), 6.96 (d, J = 7.4 Hz, 1 H), 7.09–7.14 (m, 2 H), 7.29 (t, 7.4 Hz, 1 H), 7.52-7.73 (m, 8 H), 8.02 (d, J = 8.2 Hz, 1 H), 8.08–8.18 (m, 3 H), 8.38 (d, J = 4.0 Hz, 1 H), 8.69 (s, 1 H). ^{13}C NMR (DMSO-d_6, 125 MHz, ppm): δ 162.5, 149.3, 147.6, 147.4, 147.2, 145.8, 141.3, 139.7, 139.3, 136.3, 134.0, 130.8, 130.5, 129.7, 128.5, 128.3, 128.1, 127.3, 126.6, 125.4, 125.1, 124.6, 124.4, 123.9, 123.1, 121.6, 119.3, 117.7, 117.3, 115.6, 99.0, 33.8, 29.5, 29.4. FAB MS: *m/z* 684.2 [M^+]. HRMS: Calcd for $C_{46}H_{40}O_2N_2S$: 684.2811. Found: 684.2811 [M^+].

2.6. 5′-(2,6-Di-tert-butyl-10-(naphthalen-1-yl(phenyl)amino) anthracen-9-yl)-2,2′-bithiophene-5-carbaldehyde (**6**)

A tetrahydrofuran (50 ml) solution of compound **3** (1.17 g, 2.0 mmol) was cooled to −70 °C and *n*-butyl lithium (1.4 ml (1.6 M solution in *n*-hexane) 2.2 mmol) was added dropwise for 15 min with vigorous stirring. The reaction mixture was stirred for another 60 min at this temperature and 0.72 g (2.2 mmol) of tributylchlorostannane added at once. The resulting solution was allowed to attain room temperature overnight. It was quenched by the addition of ice-cold water and extracted with diethyl ether (3 × 30 ml). The combined organic extracts was dried over anhydrous $MgSO_4$ and evaporated to yield orange syrup.

The above syrup was mixed with 5-bromothiophene-2-carbaldehyde (0.38 g, 2.0 mmol), $Pd(PPh_3)_2Cl_2$ (0.014 g, 0.02 mmol) and dimethylformamide (10 ml) and heated at 70 °C for 24 h. The reaction was quenched by cooling to room temperature and subsequently 20 ml methanol added to induce precipitation of the product. The yellow solid thus obtained was dissolved in dichloromethane and adsorbed with silica gel. It was purified by column chromatography using hexane/dichloromethane mixture (3:2) as eluant. Dark yellow solid. Yield: 1.04 g (74%). ^{1}H NMR ($CDCl_3$, 500 MHz, ppm): δ 1.10 (s, 9 H), 1.31 (s, 9 H), 6.70–6.74 (m, 2 H), 6.84 (t, J = 8.2 Hz, 1 H), 7.05–7.14 (m, 3 H), 7.18–7.27 (m, 2 H), 7.35 (d, J = 4.0 Hz, 1 H), 7.40–7.56 (m, 4 H), 7.60–7.64 (m, 2 H), 7.71 (d, J = 4.0 Hz, 1 H), 7.88–7.98 (m, 3 H), 8.21–8.26 (m, 2 H0, 8.32 (d, J = 8.2 Hz, 1 H), 9.92 (s, 1 H). ^{13}C NMR ($CDCl_3$, 125 MHz, ppm): δ 182.5, 150.7, 148.4, 148.0, 147.7, 147.2, 142.8, 141.8, 141.6, 140.8, 137.4, 137.2, 135.2, 132.4, 131.5, 130.8, 130.3, 129.7, 129.0, 129.0, 128.3, 126.4, 126.3, 126.28, 126.1, 125.9, 125.8, 125.7, 125.6, 125.3, 125.1, 124.4, 124.2, 123.7, 123.2, 123.0, 121.0, 119.8, 119.4, 118.6, 35.0, 30.7. FAB MS: *m/z* 699.2 [M^+]. HRMS: Calcd. for $C_{47}H_{41}ONS_2$: 699.2630. Found: 699.2629 [M^+].

2.7. (E)-2-Cyano-3-(5′-(2,6-di-tert-butyl-10-(naphthalen-1-yl (phenyl)amino)anthracen-9-yl)-2,2′-bithiophen-5-yl)acrylic acid (**7**)

The title dye was prepared from the aldehyde **6** by following the procedure described above for **5**. Red solid. Yield: 77%. ^{1}H NMR (DMSO-d_6, 500 MHz, ppm): δ 0.95 (s, 9 H), 1.17 (s, 9 H), 6.49 (d, J = 7.4 Hz, 1 H), 6.56 (d, J = 7.4 Hz, 1 H), 6.75–6.79 (m, 1 H), 6.96 (d, J = 7.4 Hz, 1 H), 7.03–7.07 (m, 2 H), 7.21 (t, J = 7.4 Hz, 1 H), 7.35 (d, J = 1.8 Hz, 1 H), 7.45–7.67 (m, 6 H), 7.79–7.82 (m, 3 H), 7.96–7.98 (m, 2 H), 8.07–8.14 (m, 3 H), 8.51 (s, 1 H). ^{13}C NMR (DMSO-d_6, 125 MHz, ppm): δ 164.0, 150.7, 148.9, 148.4, 146.6, 145.5, 142.6, 141.5, 140.8, 140.7, 137.0, 135.3, 134.7, 132.2, 132.17, 131.3, 129.8, 129.6, 129.5, 128.7, 127.9, 127.7, 126.8, 126.4, 126.3, 125.73, 125.66, 125.2, 124.4, 122.9, 120.9, 120.5, 119.0, 118.5, 117.0, 99.2, 35.1, 30.8, 30.7. FAB MS: *m/z* 766.3 [M^+]. HRMS: Calcd. for $C_{50}H_{42}O_2N_2S_2$: 766.2688. Found: 766.2693 [M^+].

2.8. 5-(7-(5-(2,6-Di-tert-butyl-10-(naphthalen-1-yl(phenyl)amino) anthracen-9-yl)thiophen-2-yl)benzo[c][1,2,5]thiadiazol-4-yl) thiophene-2-carbaldehyde (**8**)

It was obtained in 72% yield as described above for the aldehyde **6**, but 5-(7-bromobenzo[*c*][1,2,5]thiadiazol-4-yl)thiophene-2-carbaldehyde was used instead of 5-bromothiophene-2-carbaldehyde. Orange solid. ^{1}H NMR ($CDCl_3$, 500 MHz, ppm): δ 1.09 (s, 9 H), 1.29 (s, 9 H), 6.70–6.74 (m, 2 H), 6.83 (t, J = 7.4 Hz, 1 H), 7.09–7.27 (m, 4 H), 7.33–7.56 (m, 5 H), 7.63 (d, J = 8.2 Hz, 1 H), 7.85 (d, J = 4.0 Hz, 1 H), 7.92–8.06 (m, 5 H), 8.21–8.25 (m, 3 H), 8.33 (d, J = 8.2 Hz, 1 H), 8.49 (d, J = 4.0 Hz, 1 H), 10.0 (s, 1 H). ^{13}C NMR ($CDCl_3$, 125 MHz, ppm): δ 183.0, 152.5, 152.45, 150.8, 148.7, 148.4, 147.9, 143.4, 142.9, 142.3, 140.6, 140.1, 136.8, 135.2, 132.5, 131.6, 130.9, 129.7, 129.0, 128.98, 128.8, 128.3, 128.0, 127.9, 127.5, 127.1, 126.7, 126.2, 125.9, 125.8, 125.7, 125.2, 125.0, 124.9, 124.4, 124.3, 123.0, 121.3, 119.8, 119.4, 118.6, 35.0, 30.8. FAB MS: *m/z* 833.3 [M^+]. HRMS: Calcd. for $C_{53}H_{43}ON_3S_3$: 833.2568. Found: 833.2575 [M^+].

2.9. (E)-2-Cyano-3-(5-(7-(5-(2,6-di-tert-butyl-10-(naphthalen-1-yl(phenyl)amino)anthracen-9-yl)thiophen-2-yl)benzo[c][1,2,5] thiadiazol-4-yl)thiophen-2-yl)acrylic acid (**9**)

It was prepared in 63% yield from the aldehyde **8** by following a procedure similar to **5**. Dark red solid. ^{1}H NMR (DMSO-d_6, 500 MHz, ppm): δ 0.98 (s, 9 H), 1.18 (s, 9 H), 6.52 (d, J = 7.4 Hz, 1 H), 6.59 (d, J = 7.4 Hz, 1 H), 6.80 (t, J = 7.4 Hz, 1 H), 6.98–7.12 (m, 3 H), 7.26–7.29 (m, 1 H), 7.47–7.57 (m, 5 H), 7.71 (d, J = 4.0 Hz, 1 H), 7.85–7.89 (m, 2 H), 8.00–8.31 (m, 8 H), 8.45–8.53 (m, 2 H). ^{13}C NMR

(DMSO-d_6, 125 MHz, ppm): δ 163.8, 151.8, 150.5, 148.7, 148.2, 147.4, 146.5, 142.5, 141.6, 140.3, 140.0, 137.1, 135.2, 132.0, 131.2, 129.6, 129.4, 128.8, 128.6, 128.3, 127.8, 127.8, 127.1 126.8, 126.5, 126.3, 126.0, 125.5, 125.1, 124.1, 123.9, 122.7, 121.0, 120.4, 118.4, 116.8, 99.2, 35.0, 30.7, 30.6. FAB MS: *m/z* 900.2 [M^+]. HRMS: Calcd. for $C_{56}H_{44}O_2N_4S_3$: 900.2626. Found: 900.2632 [M^+].

2.10. Computational details

The ground state geometries of the compounds at the gas phase were optimized by employing density functional theory with Becke three parameter hybrid functional and correlation functional of Lee, Yang, and Parr (B3LYP) and the basis set 6-31G with additional d polarization functions on first row element and p polarization functions on hydrogens (6-31G**) as implemented in the Gaussian 09 package [41]. The default options for the self-consistent field (SCF) convergence and threshold limits in the optimization were used. The vertical electronic excitations were calculated using the time-dependent DFT (B3LYP) theory and the above mentioned basis set. At least 10 excited states were calculated for each molecule. Even though the time-dependent DFT method less accurately describes the states with charge-transfer nature, the qualitative trends in the TDDFT results can still offer correct physical insights.

2.11. DSSC fabrication and characterization

The TiO_2 thin film serving as the photoanode in this work was prepared through the general sol–gel method. The precursor solution was made according to the following procedure: 430 ml of 0.1 M nitric acid solution under vigorous stirring was slowly combined with 72 ml $Ti(C_3H_7O)_4$ to form a mixture. After the hydrolysis, the mixture was heated at 85 °C in a water bath and stirred vigorously for 8 h in order to achieve the peptization. When the mixture was cooled to room temperature, the resultant colloid

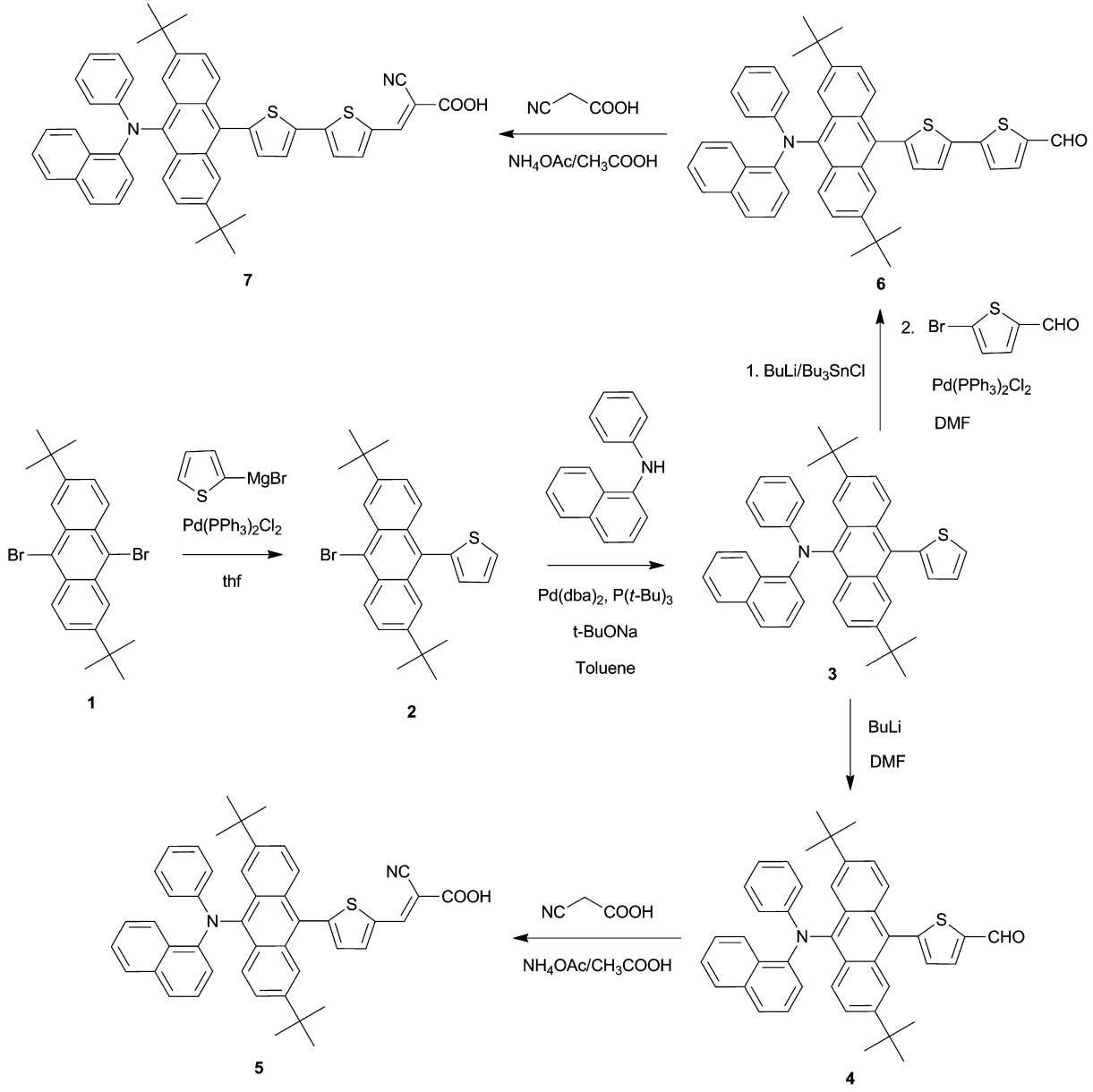

Scheme 1. Synthesis of the thiophene containing dyes **5** and **7**.

was filtered, and the filtrate was then heated in an autoclave at a temperature of 240 °C for 12 h to grow the TiO_2 particles. When the colloid was cooled to room temperature, it was ultrasonically vibrated for 10 min. The TiO_2 colloid was concentrated to 13 wt %, followed by the addition of 30 wt % (with respect to TiO_2 weight) of poly(ethylene glycol) (PEG, MW) 20,000 g/mol) to prevent the film from cracking while drying.

The TiO_2 paste was then deposited on a FTO glass substrate by the glass rod method. The TiO_2-coated FTO was heated to 500 °C at a heating rate of 20 °C/min. and maintained for 30 min before being cooled to room temperature. The thickness of TiO_2 film was controlled by repeating the procedure described above. The thickness and the area of TiO_2 film were controlled at 18 μm and 3 cm^2, respectively. The TiO_2 film thickness was measured by a profilometer (Dektak3, Veeco/Sloan Instruments Inc., USA). The illumination area was constrained using a cardboard mask. A platinized FTO with a layer of Pt 100 nm-thick applied by sputtering was used as a counter electrode. The active area was controlled at a dimension of 0.5×0.5 cm^2 by adhered polyester tape (3 M) with a thickness of 60 μm on the Pt electrode. After heating of the TiO_2 thin film to 80 °C, the film was taken out from the oven and dipped into the THF solution containing 3×10^{-4} M dye sensitizers for at least 12 h. Use of THF solution for dipping was meant to ensure enough uptakes of the sensitizers due to the higher solubility of the sensitizers in THF. After being rinsed with CH_3CN, the photoanode was placed on top of the counter electrode and tightly clipped to it to form a cell. Electrolyte was then injected into the space and the cell sealed with Torr Seal cement (Varian, MA). The electrolyte was composed of 0.5 M lithium iodide (LiI), 0.05 M iodine (I_2), and 0.5 M 4-*tert*-butylpyridine dissolved in acetonitrile. Note that there was no mask used to constrain the illumination area of the device in this study; therefore, the power conversion efficiency and the corresponding measurements might be overestimated [42]. However, our results were compared with that of N3 dye (*cis*-bis (4,4′-dicarboxy-2, 2′-bipyridine) dithiocyanato ruthenium (II)) [43], which acted as a reference for each measurement, and the conditions for each device were identical. Therefore, we believe that the difference of the performance among the devices made in this study was mainly attributed to the intrinsic properties of the sensitizers.

The photoelectrochemical characterizations on the solar cells were carried out using a modified light source, 300W Xe lamp (Oriel, 6258) equipped with a water-based IR filter and AM 1.5 filter (Oriel, 81080 kit). Light intensity, attenuated by neutral density filter (Optosigma, 078-0360) at the measuring (cell) position, was estimated to be *ca.* 100 mW/cm^2 according to the reading from a radiant power meter (Oriel, 70310) connected to a thermopile probe (Oriel, 71964). Photoelectrochemical characteristics of the DSSCs, were recorded through the potentiostat/galvanostat (CHI650B, CH Instruments, Inc., USA).

3. Results and discussion

3.1. Synthesis and characterization

The synthetic methods employed to obtain the dyes (Fig. 1) are shown in Schemes 1 and 2. In the first step the dibromo derivative of anthracene **1** was treated with thienylmagnesium bromide in the presence of $Pd(PPh_3)_2Cl_2$ in tetrahydrofuran to obtain the thiophene derivative **2** in 56% yield. It was converted to the amine substituted compound **3** by treatment with *N*-phenylnaphthalen-1-amine under the palladium catalyzed ($Pd(dba)_2$/(*t*-Bu)$_3$P) C-N cross coupling conditions [44] in 81% yield. Compound **3** was then converted to the corresponding aldehyde, **4** by reacting with *n*-butyl lithium followed by dry dimethylformamide. The aldehydes **6** and **9** were accessed by condensing the stannylene derivative of **3** with either 2-bromo-5-thiophene aldehyde or 5-(7-bromobenzo [*c*][1,2,5]thiadiazol-4-yl)thiophene-2-carbaldehyde by following the Stille coupling protocol and $Pd(PPh_3)_2Cl_2$/dmf reagent system [45]. In the final step, the aldehyde precursors (**4**, **6** and **8**) were successfully converted to the desired dyes (**5**, **7** and **9**) on treatment with cyanoacetic acid in the presence of ammonium acetate catalyst in acetic acid. The dyes are deep red in colour and soluble in common organic solvents such as dichloromethane, tetrahydrofuran and methanol.

3.2. Optical properties

A dye suitable for application in dye-sensitized solar cell must possess a broad absorption profile covering the entire visible region. In order to determine the optical absorption of the dyes we have

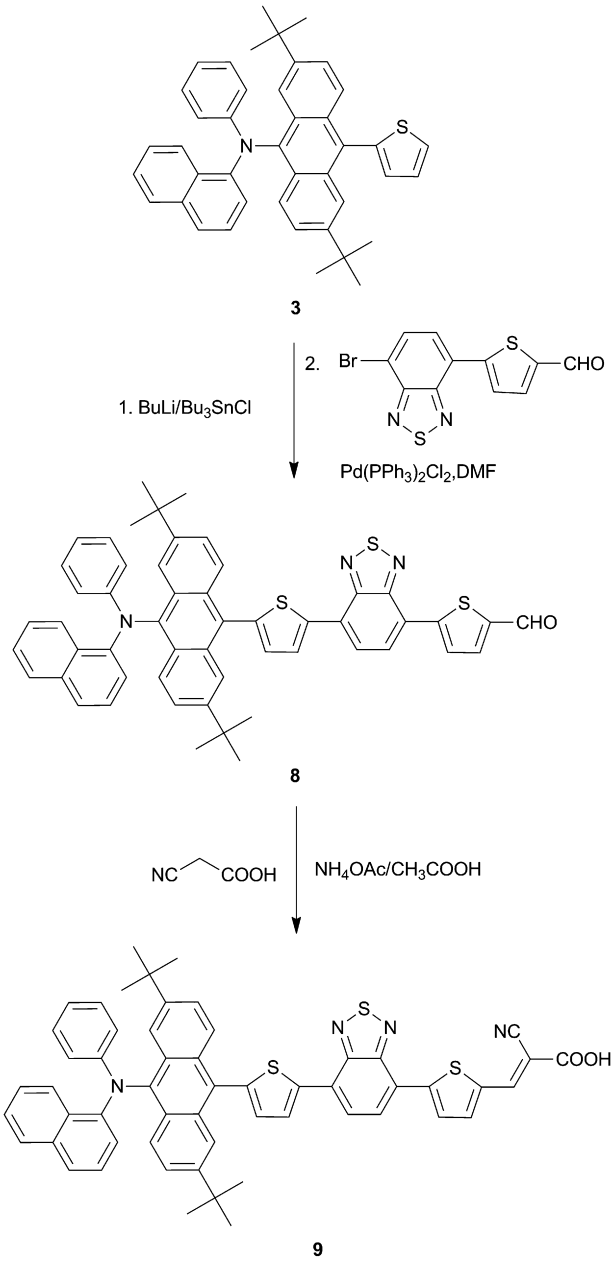

Scheme 2. Synthesis of the benzothiadiazole containing dye **9**.

Table 1
Optical and electrochemical data of the dyes.

Dye	λ_{abs}, nm (ε_{max}, $\times 10^{+4}$ M^{-1} cm^{-1})		λ_{em},[a] nm (Φ_f)	Stokes shift,[a] cm^{-1}	E_{ox}, V (ΔE_p, mV)	HOMO, eV	LUMO, eV	$E_{0\text{-}0}$, eV	$E_{0\text{-}0}^*$, eV
	THF	CH_2Cl_2							
3	–	425 (1.11), 357 (1.09)	–	–	0.466 (81), 0.554 (120)	5.266	2.628	2.638	–
5	434 (1.31), 344 (2.50)	435(1.28), 350 (2.72)	508 (0.12)	3356	0.604 (73), 0.770 (83)	5.404	2.949	2.455	−1.08
7	436 (3.58), 366(sh)	442 (4.10), 364 (sh)	565 (0.07)	5237	0.496 (63)	5.296	2.912	2.384	−1.12
9	486 (3.94), 366 (2.26)	491 (4.49), 365 (2.12)	633 (0.02)	4778	0.451 (60)[b]	5.251	3.150	2.101	−0.88

[a] Recorded for tetrahydrofuran solutions. Coumarin-6 or Rhodamine-6G (for **7** and **9**) was used as standards in the quantum yield measurements.
[b] An additional reversible reduction couple was observed at −1.612 (66) which is attributable to the reduction of the benzothiadiazole segment.

performed the electronic spectral measurements in dichloromethane and tetrahydrofuran. The optical parameters deduced from the absorption studies are listed in Table 1 and the absorption spectra recorded for the dichloromethane solutions of the dyes (**5**, **7**, and **9**) and the selected precursors (**3** and **6**) are displayed in Fig. 2.

The absorption profile of the parent amine (**3**) displays two peaks centred at 425 and 357 nm respectively (Fig. 2). On introducing the acceptor group the higher wavelength band grows in intensity with a significant red-shift while the higher energy peak remains unaltered except for a slight hike in molar extinction coefficient. Presence of higher wavelength electronic transitions in the parent amine (**3**) overrules the possibility of pure charge transfer character to the second absorption observed for the dyes. However, it is likely that the peak at 425 nm in the precursor compound (**3**) originates from the charge transfer from amine functionality to the π^* orbitals of the anthracene segment. Such an intramolecular charge transfer (ICT) electronic excitation is commonly observed in amine derivatives of polyaromatics [46,47].

In the dyes, the higher wavelength (434–486 nm) absorption may also possess contribution from a charge transfer from the amine to the acceptor segment. This peak is slightly red-shifted for the bithiophene derivative (**7**) and moved to 486 nm for the dye (**9**) containing the dithienylbenzothiadiazole bridge. This clearly points that benzothiadiazole being a low-band gap chromophore significantly alters the electronic structure of the dye and reduces the band gap tremendously by lowering the LUMO energy level (*vide infra*) [24]. The molar extinction coefficient of the dye **7** is three times larger than that observed for the compound **5**. The extension of the linker conjugation in dipolar compounds is expected to diminish the donor–acceptor interaction and consequently reduce the absorption intensity of the peak arising due to the charge transfer transition [20]. However, the enormous increase in the molar extinction coefficient for the dye **7** when compared to **5** is probably pointing the presence of a significant π–π^* contribution to this profile or an enhanced donor–acceptor interaction mediated through the conjugation bridge. Alternatively, an increment in the donor strength due to the addition of thiophene unit may attenuate the donor–acceptor interaction. A broadening observed for this transition on increasing the spacer length also suggests the involvement of additional electronic transitions rather than a straightforward donor to acceptor-based transition.

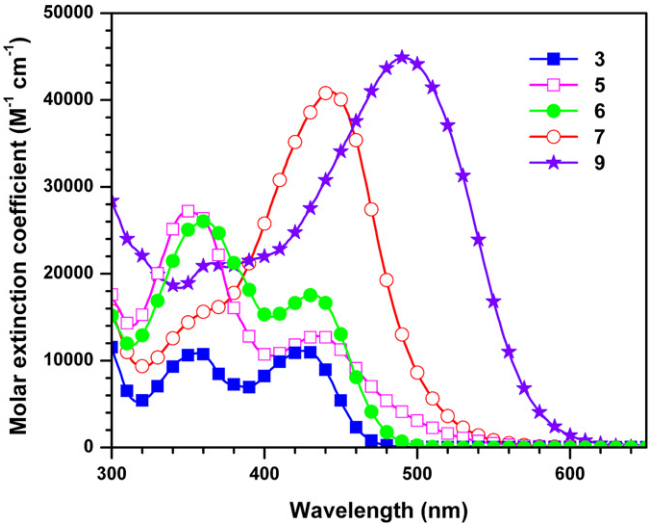

Fig. 2. Absorption spectra of the dyes **5**, **7**, and **9** along with the precursors **3** and **6** recorded in dichloromethane.

It is interesting to compare the optical properties of the dyes with the related compounds containing fluorene [10,22] or phenyl [5] segments in place of anthracene (Table 2). Firstly, the anthracene derivative, **5** possesses red-shifted absorption when compared to the analogous fluorene (**10**, +14 nm) and phenyl (**12**, +31 nm) derivatives, however, with the moderate optical density. Such a lowering of absorption energy indicates the involvement orbital based on anthracene in the absorption rather than an orbital based on cyanoacrylic acid segment. Relatively, anthracenes are expected to exert more stabilizing effect on the unoccupied molecular orbitals when compared to the phenyl and fluorene segments due to the π-acceptor ability. Secondly, in the fluorene and phenyl derivatives [5,7,10,22] (see Table 2) the absorption peak is bathochromically shifted on increasing the conjugation by the insertion of the thiophene moiety (compare **10** and **12** with **11** and **13** respectively). However, in the present compounds addition of thiophene exerts only a slight effect on the absorption position (compare **5** with **7**). This clearly indicates that the orbitals involved in the electronic transitions corresponding to this peak are localized within anthracene and are less influenced by the thiophene unit.

In addition, all the dyes exhibit a lower wavelength absorption peak at ca. 350 nm which is insensitive to the alternations in the structure of the dyes. It is likely to originate from the anthracene localized π–π^* transition.

In order to gain more insights into the nature of electronic transitions and the orbitals contributing to the transitions we have performed the TDDFT [48] computations on the DFT [49] optimized structures. The low energy vertical transitions predicted by the TDDFT computations and their orbital contributions are collected in Table 3. In order to access the impact of the electron-withdrawing cyanoacrylic acid on the electronic structure we have also performed calculations on the precursors **3** and **4**. The HOMO and LUMO are localized on the triarylamine and anthracene segments respectively in these compounds. In the compound **4**, the LUMO + 1 is mainly composed by the thiophene and aldehyde segments. However, in the dyes **5**, **7** and **9** the HOMO and LUMO orbitals are localized on the triarylamine and acceptor segments respectively (Fig. 3). The HOMO-1 in these dyes is again composed of the triarylamine unit. The LUMO + 1 is located on the anthracene segment for the dyes **5** and **7** and is contributed by the acceptor unit in the dye **9**. The segment wise contributions to the construction of the orbitals, LUMO and LUMO + 1 clearly establish the electronic

Table 2
Optical and electrochemical parameters of the related dyes.

Dye	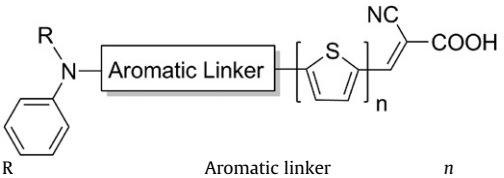			λ_{max}, nm (ε_{max}, $\times 10^{+4}$ M^{-1} cm^{-1})	E_{ox}, V	HOMO/LUMO, eV	$E_{0\text{-}0}$, eV	$E_{0\text{-}0}^{*}$, eV	Ref
	R	Aromatic linker	*n*						
10	1-naphthyl	9,9-diethyl fluorene	1	421 (5.29), 333 (1.39)[a]	0.51	5.31/2.81	2.51	−1.23	10
11	1-naphthyl	9,9-diethyl fluorene	2	470 (5.00), 363 (3.00)[a]	0.46, 0.75	5.26/3.07	2.19	0.96	6
12	Phenyl	Benzene	1	404 (2.50)	1.21 *vs* NHE		2.64	−1.43	5
13	Phenyl	Benzene	2	473 (4.35), 351 (1.79), 302 (2.15)[a]	0.49	5.29/3.09	2.20	−0.96	14
				461(2.71)[b]	0.79[b]	5.29/2.99	2.30		7
14	Phenyl	Benzene	3	480 (4.62), 386 (2.24), 302 (2.07)[a]	0.43, 0.57	5.23/3.06	2.17	−0.97	14
15	1-naphthyl	Benzene	2	461 (3.13)[b]	0.81[b]	5.31/2.99	2.32	–	7
16	Phenyl	Thiophene	2	468 (2.25)[b]	0.58[b]	5.08/2.84	2.24	–	7
17	1-naphthyl	Thiophene	2	480 (2.22)[b]	0.53[b]	5.03/2.87	2.16	–	7

[a] Recorded for dichloromethane solutions.
[b] Recorded for tetrahydrofuran solutions.

impact of the acceptor segments. Introduction of the electron-accepting cyanoacrylic acid first shifts the LUMO from the anthracene segment (compare **3**, **4**, **5** and **7**) to the cyanoacrylic acid unit. However, its accepting ability is not enough to adopt the LUMO + 1. Addition of benzothiadiazole alters the electronic structure and pushes the LUMO + 1 to the acceptor end.

The higher wavelength vertical transitions predicted by the theory for the precursors **3** and **4** possess major contribution from the HOMO to LUMO electronic excitation and possess very large oscillator strength. But in the dyes **5**, **7** and **9** HOMO to LUMO transitions have very low oscillator strength (<0.1) and are not observable in the experimental spectra. However, the peaks appearing at the next lower wavelengths (493, 499 and 555 nm) with reasonable intensity reveal major contributions from HOMO-1 to LUMO and HOMO to LUMO + 1 transitions for the dyes **5** and **7** while it is originating from the HOMO-2 to LUMO transition for the dye **9**. From the nature of the orbitals, it is clearly evident that the absorption peaks of the dyes **5** and **7** occurring at 435 and 442 nm respectively in dichloromethane solutions are originating from the $\pi-\pi^*$ and charge transfer transitions. On the contrary in the compound **9** the peak at 491 nm is attributed to the charge transfer transition involving the triarylamine donor and benzothiadiazole based acceptor moieties. The wavelength order of the red region absorption for the compounds is **3** < **4** < **5** ~ **7** < **9**, which is in keeping with the theoretical predictions. The trend in the absorption intensity realized for the dyes (**5** < **7** < **9**) is also roughly matching with the proposed trend. Thus, the highly intense and red-shifted absorption profile observed for the dye **9** is quite expected from the theoretical computations. However, a slight overestimation (+50 nm) of absorption wavelengths for the dyes at the TDDFT level is attributed to the flaws in modelling the long range charge transfer interactions.

The dyes are weakly emissive in tetrahydrofuran but the fluorescence is completely quenched when measured in dichloromethane. This is probably due to the intramolecular electron-transfer quenching or dipole-dipole interactions present in the more polar solvent. The fluorescence behaviour of the dyes in nonpolar solvents such as toluene or hexane could not be determined due to their poor solubility.

3.3. Electrochemical properties

For an efficient electron injection to the TiO_2 electrode, the dyes must possess excited state potential lower than the conduction-band-edge energy of the photoanode. Such an electronic arrangement will benefit a favourable down-hill electron conduction process. The dye regeneration is essential to achieve high stability and operational lifetime for the DSSCs. Efficient dye regeneration is possible only if the ground state redox potential of the dye is more positive than that of the electrolyte. As the excited state oxidation potential can be grossly estimated from the ground state oxidation potential and the energy gap, we have evaluated the redox behaviour of the dyes in dichloromethane using the conventional three-electrode cell assembly and cyclic voltammetric technique. It is expected to throw information about the nature of oxidation process resulting in the electron injection to the TiO_2

Table 3
Computed (TDDFT/6-31G(d,p)/B3LYP) vertical transitions, their compositions, orbital energies and dipole moments.

Compound	λ_{abs}, nm	*f*	Assignment	HOMO, eV	LUMO, eV	μ_g, Debye
3	480	0.13	HOMO → LUMO (89%) HOMO-1 → LUMO (10%)	−4.869	−1.797	0.38
4	489	0.13	HOMO → LUMO (90%) HOMO-1 → LUMO (8%)	−5.009	−1.970	3.83
5	634	0.003	HOMO → LUMO (96%)	−5.136	−2.768	8.93
	505	0.007	HOMO-1 → LUMO (86%) HOMO → LUMO + 1 (9%)			
	499	0.12	HOMO → LUMO + 1 (84%) HOMO-1 → LUMO (9%) HOMO-1 → LUMO + 1 (5%)			
7	628	0.001	HOMO → LUMO (98%)	−5.055	−2.750	7.50
	493	0.18	HOMO → LUMO + 1 (58%) HOMO-1 → LUMO (34%) HOMO-1 → LUMO + 1 (5%)			
	492	0.11	HOMO-1 → LUMO (64%) HOMO → LUMO + 1 (32%)			
9	772	0.003	HOMO → LUMO (98%)	−5.025	−3.123	8.50
	581	0.008	HOMO-1 → LUMO (98%)			
	555	1.05	HOMO-2 → LUMO (94%)			

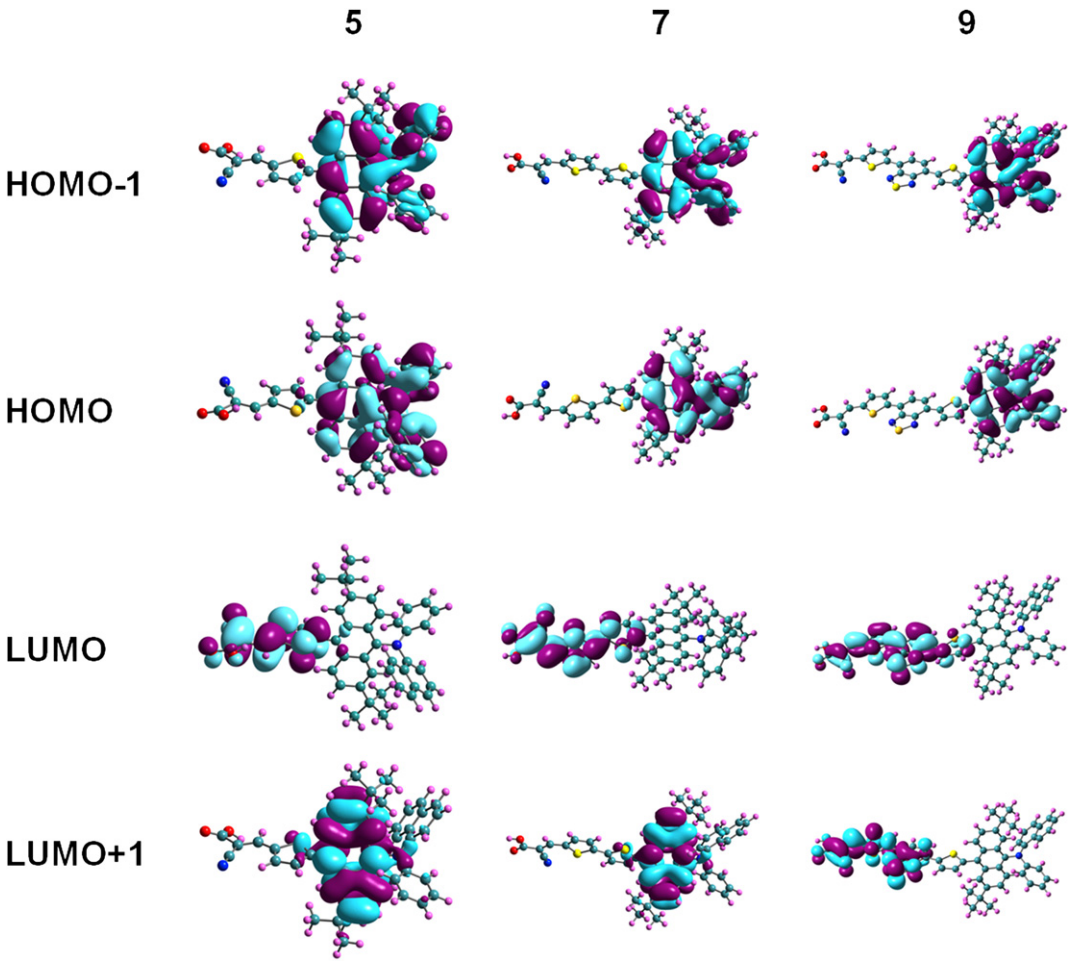

Fig. 3. Molecular orbital diagrams of the dyes calculated by TDDFT (B3LYP-6-31G(d,p)) method.

photoanode and the regeneration feasibility by electron acceptance from the electrolyte.

All the dyes exhibited a quasi reversible oxidation process in the potential range 0.60–0.45 V *vs.* the internal ferrocene/ferrocenium couple (Fig. 4). Firstly, for the dyes reported here, the oxidation potentials lie in the range 1.22–1.37 V *vs* NHE. These values are anodically shifted to that of the electrolyte (I^-/I_3^-) redox couple (~0.4 V *vs* NHE) and suggest facile dye regeneration in the presence of electrolyte. Secondly, the quasi-reversibility observed for the redox potential arising due to the oxidation of the amine functionality attests the electrochemical robustness of the dyes. Thirdly, the excited state oxidation potential deduced for the dyes (−0.88 to −1.12 V vs NHE) are more negative than the conduction-band-edge energy level of the TiO_2 electrode (−0.5 V *vs* NHE) [12]. This suggests that an electron injection from the dyes to TiO_2 photoanode is favourable.

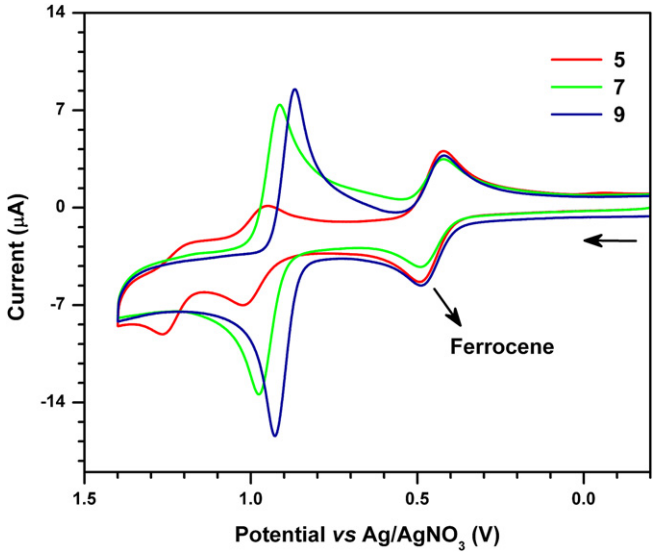

Fig. 4. Cyclic voltammograms recorded for the dyes **5**, **7**, and **9** in dichloromethane.

The oxidation potential of the dyes decreases in the order, **5** > **7** > **9**. In compound **7**, incorporation of additional thiophene unit in the conjugation pathway may increase the electron-richness of the aromatic linker which in turn facilitates the oxidation of the end-capped amine unit [8]. On the contrary, an anodically shifted redox potential observed for the dye containing the electron-accepting benzothiadiazole segment (**9**) in the conjugation is interesting. It may be argued that the extension of conjugation length between the amine donor and the cyanoacrylic acid acceptor

Table 4
Performance characteristics of the dye-sensitized solar cells.

Dye	J_{sc} (mA/cm^2)	V_{oc} (V)	*FF*	η (%)
5	6.00	0.565	0.648	2.20
7	8.28	0.535	0.657	2.91
9	9.80	0.520	0.633	3.23
N3	18.04	0.741	0.589	7.87

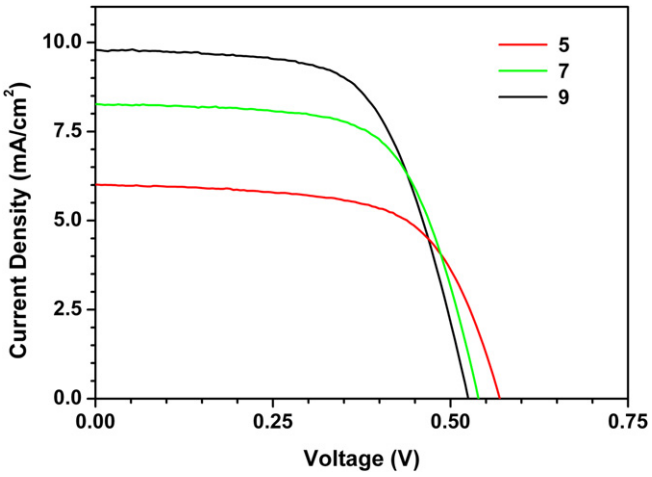

Fig. 5. I–V plots of the DSSCs constructed using the dyes **5**, **7** and **9**.

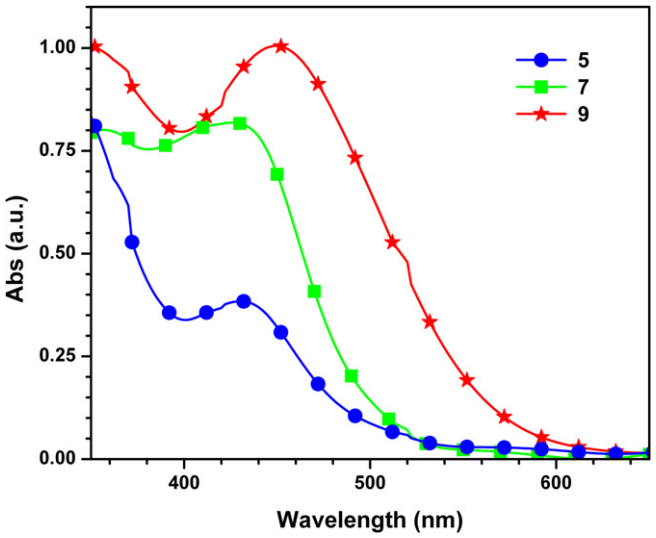

Fig. 7. Absorption spectra of the dyes **5**, **7**, and **9** anchored on nanocrystalline anatase TiO_2.

beyond a saturation limit may downgrade the electronic communication between them. An amine not so much influenced by an acceptor segment may oxidize at a lower potential than the amine affected by an acceptor group. In fact, the oxidation potential observed for this dye (**9**) is lesser than that observed for the parent amine, **3** (Table 1). This clearly points that the elongation of conjugation plays a critical role in facilitating the oxidation of the molecule rather than the effect due to the insulation of amine and acceptor units by linker extension.

The orbital energies computed (Table 3) for the dyes (**5**, **7** and **9**) are comparable to those deduced from the electrochemical data measured in the dichloromethane solutions. From the orbital energies it is evident that the incorporation of acceptor segment lowers the LUMO level and the extension of conjugation raises the HOMO level. Thus, the variation in the structural elements helps the fine tuning of the orbital energies which is expected to benefit the electron injection to the TiO_2 layer and the dye regeneration by the electrolyte. Orbital energies of the related dyes containing fluorene or phenyl segments in place of anthracene are close to those observed for the present dyes [5,7,10,22] (see Table 2).

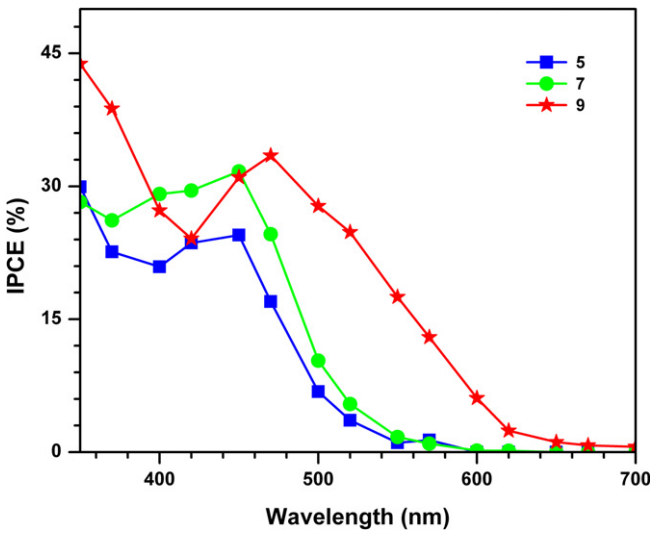

Fig. 6. IPCE plots of the DSSCs fabricated using the dyes **5**, **7**, and **9**.

3.4. DSSC characteristics

The dye-sensitized solar cells were constructed by using the dyes **5**, **7** or **9** as the sensitizer for nanocrystalline anatase TiO_2 in a conventional Grätzel photoelectrochemical cell. Typically, the effective light exposure area of the DSSCs was maintained at 0.25 cm^2, and a liquid electrolyte composed of 0.05 M I_2/0.5 M LiI/0.5 M *tert*-butylpyridine in acetonitrile solution used. The device performance statistics under AM 1.5 illumination are collected in Table 4. Fig. 5 shows the photocurrent–voltage (I–V) curves of the cells. The incident photon-to-current conversion efficiencies (IPCE) of the dyes on TiO_2 are plotted in Fig. 6. The devices of the dyes exhibited moderate conversion efficiencies, ranging from 28% to 41% of the standard device fabricated using the ruthenium dye **N3** and evaluated under identical conditions.

The order of efficiency observed for the dyes studied in this work roughly correlates well with the trend in the molar extinction coefficients for the absorption peaks realized for the dyes. The dye **5** is possessing blue-shifted and hypsochromic absorption among the series while the compound **9** displays a broad, red-shifted and hypochromic absorption. The open-circuit voltages (V_{OC}) observed for the DSSCs are in the order **5** > **7** > **9**. However, the short-circuit current (J_{sc}) measured for the DSSCs using the dyes are in the reverse order (**9** > **7** > **5**). Larger short-circuit current and open-circuit voltage and smaller overall fill factor (*FF*) are responsible for the improved efficiency realized for the **N3** dye [50]. All the dyes adsorbed on TiO_2 displayed a blue shift in the absorption spectra (~25 to 40 nm, see Fig. 7) which probably indicates the deprotonation of cyanoacrylic acid during the interaction with the semiconductor [6] or H-aggregation of the dyes on the surface of the semiconductor [51,52].

A comparison of the solar cell performance of the present dyes with the related compounds [5,7,10,22] suggests that the performance of these dyes are significantly influenced by the absorption features. In the dyes **5** and **7**, as the prominent absorption is occurring between the triarylamine and the anthracene based orbitals it is probable that the charge is trapped in anthracene segment. This will inhibit the electron injection into the conduction band of the TiO_2 as the anthracene segment is further away from the anchoring unit.

4. Conclusions

In summary, in this paper we have presented the synthesis, electro-optical properties and dye-sensitized solar cell performance of the new class of metal free organic dyes containing anthracene based triarylamine donor which is linked to the cyanoacrylic acid acceptor through a conjugation pathway composed of thiophene and benzothiadiazole units. The optical absorption of the dyes is red-shifted on extension of the conjugation pathway by the introduction of electron-rich oligothiophene or electron-deficient benzothiadiazole segments. Due to the enhanced electron-richness the oxidation potential is also shifted cathodically on insertion of thiophene and benzothiadiazole moieties in the conjugating unit. We have also showed that in this class of donor–acceptor compounds introduction of low band gap chromophore such as benzothiadiazole helps to localize the unoccupied molecular orbitals on the acceptor segment which is useful for the facile charge transfer transition. The DSSC characteristics of the dyes are improved on incorporation of bithiophene or dithienylbenzothiadiazole segments in the conjugation pathway which altered the HOMO and LUMO levels and subsequently favoured the electron-injection and recombination kinetics.

Acknowledgements

This research was supported by funding from Department of Science and Technology (DST/TSG/ME/2010/27) at New Delhi and the Indian Institute of Technology Roorkee (Initiation Grant) to KRJT.

Appendix. Supplementary information

Absorption and emission spectra of the dyes recorded in tetrahydrofuran, optimized structures of the dyes and their atomic coordinates are provided in the Supporting Information.

Supplementary data associated with this article can be found in the online version, at doi:10.1016/j.dyepig.2011.02.006.

References

[1] Grätzel M. Recent advances in sensitized mesoscopic solar cells. Acc Chem Res 2009;42:1788–98.
[2] Jang SR, Yum JH, Klein C, Kim KJ, Wagner P, Officer D, et al. High molar extinction coefficient ruthenium sensitizers for thin film dye-sensitized solar cells. J Phys Chem C 2009;113:1998–2003.
[3] O'Regan B, Grätzel M. A low-cost high-efficiency solar-cell based on dye-sensitized colloidal TiO_2 films. Nature 1991;253:737–40.
[4] Iwamoto S, Sazanami Y, Inoue M, Inoue T, Hoshi T, Shigaki K, et al. Fabrication of dye-sensitized solar cells with an open-circuit photovoltage of 1 V. Chem Sus Chem 2008;1:401–3.
[5] Hagberg DP, Marinado T, Karlsson KM, Nonomura K, Qin P, Boschloo G, et al. Tuning the HOMO and LUMO energy levels of organic chromophores for dye sensitized solar cells. J Org Chem 2007;72:9550–6.
[6] Baheti A, Tyagi P, Thomas KRJ, Hsu YC, Lin JT. Simple triarylamine-based dyes containing fluorene and biphenyl linkers for efficient dye-sensitized solar cells. J Phys Chem C 2009;113:8541–7.
[7] Chang YJ, Chow TJ. Dye-sensitized solar cell utilizing organic dyads containing triarylene conjugates. Tetrahedron 2009;65:4726–34.
[8] Chen CH, Hsu YC, Chou HH, Thomas KRJ, Lin JT, Hsu CP. Dipolar compounds containing fluorene and a heteroaromatic ring as the conjugating bridge for high-performance dye-sensitized solar cells. Chem Eur J 2010;16:3184–93.
[9] Karim MA, Cho YR, Park JS, Kim SC, Kim HJ, Lee JW, et al. Novel fluorene-based functional 'click polymers' for quasi-solid-state dye-sensitized solar cells. Chem Commun; 2008:1929–31.
[10] Thomas KRJ, Lin JT, Hsu YC, Ho KC. Organic dyes containing thienylfluorene conjugation for solar cells. Chem Commun; 2005:4098–100.
[11] Wang ZS, Cui Y, Dan-Oh Y, Kasada C, Shinpo A, Hara K. Molecular design of coumarin dyes for stable and efficient organic dye-sensitized solar cells. J Phys Chem C 2008;112:17011–7.
[12] Hara K, Sato T, Katoh R, Furube A, Ohga Y, Shinpo A, et al. Molecular design of coumarin dyes for efficient dye-sensitized solar cells. J Phys Chem B 2003;107:597–606.
[13] Li R, Lv X, Shi D, Zhou D, Cheng Y, Zhang G, et al. Dye-sensitized solar cells based on organic sensitizers with different conjugated linkers: furan, bifuran, thiophene, bithiophene, selenophene, and biselenophene. J Phys Chem C 2009;113:7469–79.
[14] Thomas KRJ, Hsu YC, Lin JT, Lee KM, Ho KC, Lai CH, et al. 2,3-Disubstituted thiophene-based organic dyes for solar cells. Chem Mater 2008;20:1830–40.
[15] Liu WH, Wu IC, Lai CH, Chou PT, Li YT, Chen CL, et al. Simple organic molecules bearing a 3,4-ethylenedioxythiophene linker for efficient dye-sensitized solar cells. Chem Commun; 2008:5152–4.
[16] Wang M, Xu M, Shi D, Li R, Gao F, Zhang G, et al. High-performance liquid and solid dye-sensitized solar cells based on a novel metal-free organic sensitizer. Adv Mater 2008;20:4460–3.
[17] Qin H, Wenger S, Xu M, Gao F, Jing X, Wang P, et al. An organic sensitizer with a fused dithienothiophene unit for efficient and stable dye-sensitized solar cells. J Am Chem Soc 2008;130:9202–3.
[18] Zhang GL, Bala H, Cheng YM, Shi D, Lv X, Yu QJ, et al. High efficiency and stable dye-sensitized solar cells with an organic chromophore featuring a binary π-conjugated spacer. Chem Commun; 2009:2198–200.
[19] Xu M, Li R, Pootrakulchote N, Shi D, Guo J, Yi Z, et al. Energy-level and molecular engineering of organic D-π-A sensitizers in dye-sensitized solar cells. J Phys Chem C 2008;112:19770–6.
[20] Li G, Jiang KL, Li YF, Li SH, Yang LM. Efficient structural modification of triphenylamine-based organic dyes for dye-sensitized solar cells. J Phys Chem C 2008;112:11591–9.
[21] Lin JT, Chen PC, Yen YS, Hsu YC, Chou HH, Yeh MCP. Organic dyes containing furan moiety for high-performance dye-sensitized solar cells. Org Lett 2009;11:97–100.
[22] Yen YS, Hsu YC, Lin JT, Chang CW, Hsu CP, Yin DJ. Pyrrole-based organic dyes for dye-sensitized solar cells. J Phys Chem C 2008;112:12557–67.
[23] Liu XZ, Zhu R, Zhang Y, Liu B, Ramakrishna S. Anionic benzothiadiazole containing polyfluorene and oligofluorene as organic sensitizers for dye-sensitized solar cells. Chem Commun; 2008:3789–91.
[24] Velusamy M, Thomas KRJ, Lin JT, Hsu YC, Ho KC. Organic dyes incorporating low-band-gap chromophores for dye-sensitized solar cells. Org Lett 2005;7:1899–902.
[25] Xia ZY, Zhang ZY, Su JH, Zhang Q, Fung KM, Lam MK, et al. Robust and highly efficient blue light-emitting hosts based on indene-substituted anthracene. J Mater Chem 2010;20:3768–74.
[26] Reddy MA, Thomas A, Srinivas K, Rao VJ, Bhanuprakash K, Sridhar B, et al. Synthesis and characterization of 9,10-bis(2-phenyl-1,3,4-oxadiazole) derivatives of anthracene: efficient n-type emitter for organic light-emitting diodes. J Mater Chem 2009;19:6172–84.
[27] Lyu YY, Kwak J, Kwon O, Lee SH, Kim D, Lee C, et al. Silicon-cored anthracene derivatives as host materials for highly efficient blue organic light-emitting devices. Adv Mater 2008;20:2820–3.
[28] Tao S, Zhou Y, Lee CS, Lee ST, Huang D, Zhang X. Highly efficient nondoped blue organic light-emitting diodes based on anthracene-triphenylamine derivatives. J Phys Chem C 2008;112:14603–6.
[29] Li ZH, Wong MS, Tao Y, Fukutani H. Ambipolar diphenylamino end-capped oligofluorenylthiophenes as excellent electron-transporting emitters. Org Lett 2007;9:3659–62.
[30] Liao YL, Lin CY, Wong KT, Hou TH, Huang WY. A novel ambipolar spirobifluorene derivative that behaves as an efficient blue-light emitter in organic light-emitting diodes. Org Lett 2007;9:4511–4.
[31] Huang TH, Lin JT, Chen LY, Lin YT, Wu CC. Dipolar dibenzothiophene SS-dioxide derivatives containing diarylamine: materials for single-layer organic light-emitting devices. Adv Mater 2006;18:602–4.
[32] Silvestri F, Marrocchi A, Seri M, Kim C, Marks TJ, Facchetti A, et al. Solution-processable low-molecular weight extended arylacetylenes: versatile p-type semiconductors for field-effect transistors and bulk heterojunction solar cells. J Am Chem Soc 2010;132:6108–23.
[33] Chung DS, Park JW, Park JH, Moon D, Kim GH, Lee HS, et al. High mobility organic single crystal transistors based on soluble triisopropylsilylethynyl anthracene derivatives. J Mater Chem 2010;20:524–30.
[34] Jung KH, Bae SY, Kim KH, Cho MJ, Lee K, Kim ZH, et al. High-mobility anthracene-based X-shaped conjugated molecules for thin film transistors. Chem Commun; 2009:5290–2.
[35] Marrocchi A, Silvestri F, Seri M, Facchetti A, Taticchi A, Marks TJ. Conjugated anthracene derivatives as donor materials for bulk heterojunction solar cells: olefinic versus acetylenic spacers. Chem Commun; 2009:1380–2.
[36] Teng C, Yang XC, Yang C, Li SF, Cheng M, Hagfeldt A, et al. Molecular design of anthracene-bridged metal-free organic dyes for efficient dye-sensitized solar cells. J Phys Chem C 2010;114:9101–10.
[37] Srinivas K, Yesudas K, Bhanuprakash K, Rao VJ, Giribabu L. A combined experimental and computational investigation of anthracene based sensitizers for dssc: comparison of cyanoacrylic and malonic acid electron withdrawing groups binding onto the TiO_2 anatase (101) surface. J Phys Chem C 2009;113:20117–26.
[38] Zhang ZL, Zhang Y, Yao DD, Bi H, Javed I, Fan Y, et al. Anthracene-arrangement-dependent emissions of crystals of 9-anthrylpyrazole derivatives. Crystal Growth Design 2009;9:5069–76.
[39] Zheng CJ, Zhao WM, Wang ZQ, Huang D, Ye J, Ou XM, et al. Highly efficient non-doped deep-blue organic light-emitting diodes based on anthracene derivatives. J Mater Chem 2010;20:1560–6.
[40] Chien CH, Chen CK, Hsu FM, Shu CF, Chou PT, Lai CH. Multifunctional deep-blue emitter comprising an anthracene core and terminal triphenylphosphine oxide groups. Adv Func Mater 2009;19:560–6.

[41] Frisch MJ, Trucks GW, Schlegel HB, Scuseria GE, Robb MA, Cheeseman JR, et al. Gaussian 09, Revision A.1. Wallingford CT; Gaussian, Inc.; 2009.
[42] Ito S, Nazeeruddin MK, Liska P, Comte P, Charvet R, Péchy P, et al. Photovoltaic characterization of dye-sensitized solar cells: effect of device masking on conversion efficiency. Prog Photovoltaics 2006;14:589–601.
[43] Nazeeruddin MK, Kay M, Rodicio I, Humphry-Baker R, Mueller E, Liska P, et al. Conversion of light to electricity by *cis*-X_2bis(2,2′-bipyridyl-4,4′-dicarboxylate)-ruthenium(II) charge-transfer sensitizers ($X = Cl^-$, Br^-, I^-, CN^-, and SCN^-) on nanocrystalline titanium dioxide electrodes. J Am Chem Soc 1993;115:6382–90.
[44] Hartwig JF, Kawatsura M, Hauck SI, Shaughnessy KH, Alcazar-Roman LM. Room-temperature palladium-catalyzed amination of aryl bromides and chlorides and extended scope of aromatic C–N bond formation with a commercial ligand. J Org Chem 1999;64:5575–80.
[45] Stille JK. The palladium-catalyzed cross-coupling reactions of organotin reagents with organic electrophiles. Angew Chem Int Ed 1986;25:508–23.
[46] Lockard JV, Ricks AB, Co DT, Wasielewski MR. Interrogating the intramolecular charge-transfer state of a julolidine-anthracene donor–acceptor molecule with femtosecond stimulated raman spectroscopy. J Phys Chem Lett 2010;1:215–8.
[47] Yang JS, Chiou SY, Liau KL. Fluorescence enhancement of trans-4-aminostilbene by N-phenyl substitutions: the amino conjugation effect. J Am Chem Soc 2002;124:2518–27.
[48] Marques MAL, Gross EKU. Time-dependent density functional theory. Ann Rev Phys Chem 2004;55:427–55.
[49] Parr RG, Yang WT. Density-functional theory of the electronic-structure of molecules. Ann Rev Phys Chem 1995;46:701–28.
[50] Nazeeruddin MK, Kay A, Rodicio I, Humphry-Baker R, Muller E, Liska P, et al. Conversion of light to electricity by cis-X_2bis(2,2′-bipyridyl-4,4′-dicarboxylate)ruthenium(ii) charge-transfer sensitizers ($X = Cl^-$ Br^- I^- CN^- and SCN^-) on nanocrystalline TiO2 electrodes. J Am Chem Soc 1993;115:6382–90.
[51] Mann JR, Gannon MK, Fitzgibbons TC, Detty MR, Watson DF. Optimizing the photocurrent efficiency of dye-sensitized solar cells through the controlled aggregation of chalcogenoxanthylium dyes on nanocrystalline titania films. J Phys Chem C 2008;112:13057–61.
[52] Bujdák J, Iyi N. Molecular orientation of rhodamine dyes on surfaces of layered silicates. J Phys Chem B 2005;109:4608–15.